Constraining Magma Evolution Mechanisms along the Galápagos Spreading Center between 102°W and 82°W through Trace Element Geochemistry

Senior Thesis

Submitted in partial fulfillment of the requirements for the

Bachelor of Science Degree

At The Ohio State University

By

Adam Green

The Ohio State University

2018

Approved by

Michael Barton

Dr. Michael Barton, Advisor

School of Earth Sciences

TABLE OF CONTENTS

Abstract……..ii

Acknowledgements……iii

List of Figures……...…….v

List of Tables……..vi

Introduction……...1

Geologic Setting……..……2

Methods…….3

Results

Trace Elements ……..……..……6

Major Oxides……...…….……..12

Discussion

Trace Elements and Major Oxides……...…….14

Conclusions……...……17

Suggestions for Future Research……..……..19

References Cited…..……..……..…….20

Appendix……..……..20

ABSTRACT

Past studies have been done on the Galápagos Spreading Center ridge to examine the effects of magma evolution with proximity to mantle plumes. However, these studies have not constrained the processes responsible for magma evolution along the entirety of the GSC ridge system. Using data from samples previously collected and analyzed for geochemical composition, the processes of magma evolution were constrained for the GSC. This study aimed to determine the different evolutionary processes of the GSC by focusing on trace element geochemistry. Trace element concentrations were chosen from their ability to provide insight to the natural processes driving the evolution of magmas erupted along mid-ocean ridges. Variations of trace element concentrations identified the extent of crust-magma interaction, determined bulk mantle compositions with respect to an average Normal Mid-Ocean Ridge Basalt (MORB), constrained regions of mantle plume influence on magmas, and identified discontinuous mantle source regions. Trace element spider diagrams reveal the Galápagos plume effects the GSC between 95.5°W & 86.5°W with the maximum degree of influence at 90.5°W. Trace element and major oxide behavior show fractional crystallization and crustal assimilation has occurred along the entire GSC. Plagioclase, olivine, and pyroxene play an important role in the fractional crystallization along the ridge. Magmas erupted at the GSC evolved from different mantle sources. The results from this study can further understanding of magma plumbing systems in areas with mantle plumes influencing magmas and ridges with transform fault offsets.

ACKNOWLEDGEMENTS

First off, I would like to thank the Ohio State University School of Earth Sciences (SES) for the opportunity to further develop myself as a student and a young professional. The SES has continually given me the resources to pursue my quest for knowledge as well as surrounded me with like-minded peers and advisors. This relationship with the School has been pivotal in my personal growth by fostering connections with alumni and faculty, providing numerous occasions to further my public speaking and presenting skills, and creating lifelong friendships beyond the classroom walls.

Also, many thanks to the Shell Exploration and Production Company for their funding and support of the SURE internship program. During the summer of 2017, I was fortunate enough to be accepted into the program to further my research. Through this internship I was given the much-needed time to analyze and interpret my results with the support of additional advisors and fellow researchers. I am very fortunate to have had the ability to interact with my peers and advisors who provided me with different perspectives, support, and guidance along the way. The SURE program supported my professional development through workshops and presentations, substantially improving the quality of my research.

None of my work would have been possible without the help of many incredible people from SES. I would like to start out by thanking my advisor, Dr. Michael Barton, for being my Sherpa throughout the journey that is research. I am forever thankful for the guidance, clarification, laughs, and memories shared along the way. Life has thrown me many curveballs throughout this process and without him, navigating this would have been impossible. I cannot thank Katherine Haines enough for her support and influence on this research as well as on my collegiate career. She encouraged me to follow my love for the natural world by pursuing a degree within the School of Earth Sciences. Also, I am very grateful for Ken Peterman and Jameson Scott for their wealth of knowledge and recommendations. Many thanks to Seth Bryson for being a fantastic friend, both inside and outside the classroom. I treasure all the friendly debates, support, and laughs we shared along the college journey. I would also like to thank Dr. Anne Carey and Dr. Derek Sawyer for their patience and assistance during my SURE internship, in my professional development, and throughout my undergraduate career.

Last but certainly not least, I would like to thank my friends and family for their unconditional support, encouragement, and belief in me. No matter where I am or what I am pursuing, I am extremely grateful that I have people that push me to follow my dreams and interests.

Thank you for believing in me and for inspiring me to get better daily. I would not be the person I am today without all your help. I am truly blessed to have people like you in my life.

I cannot adequately express how thankful I am to everyone that has helped me throughout the entirety of my life. This would not have been possible without you. Thank you.

LIST OF FIGURES

1. Sample locations on GSC map
2. Ridge segments with labels
3. Trace element spider diagrams ridges A–D
4. Trace element spider diagrams ridges E–I
5. Cr_N plotted against longitude
6. Sr_N plotted against longitude
7. U_N plotted against longitude
8. Trace element ratios plotted against longitude
9. K_2O plotted against TiO_2 and P_2O_5
10. K_2O and MgO plotted against longitude
11. Ridge E separated spider diagrams
12. Ba plotted against La and Nb
13. SiO_2 plotted against MgO

A1. Spreading rates plotted against longitude
A2. Ridge depths plotted against longitude
A3. K/Ti plotted against longitude
A4. K/P plotted against longitude

List of Tables

A1. Ridge segment properties

INTRODUCTION

The mid-ocean ridge system extends over 60,000 km, wrapping around the Earth like seams around a baseball. The system is composed of a continuous subaqueous mountain chain, located between diverging tectonic plates that make up the Earth's crust (Gale et al., 2013). Mid-ocean ridges generate new oceanic crust as ascending molten rock from the mantle rises to the surface and cools between two or more tectonic plates. The newly formed lithospheric plates spread away from the ridge at speeds typically between 10 mm/y and 170 mm/y, a contributing factor to the ridge's morphology. Fast-spreading ridges (>90 mm/y) are characterized by axial highs, where the seafloor is elevated by several hundreds of meters. Slow-spreading ridges (10-40 mm/y) are often marked by a deep rift valley, 1 – 3 km in depth. The rate of magma supply to these boundaries is another factor influencing ridge morphology. Axial highs may be found in areas of slow-spreading ridges if the magma supply rate is very high (Macdonald, 2001). This thesis focuses on the Galápagos Spreading Center (GSC) ridge system.

The GSC is an intermediate spreading ridge system with an average spreading rate of 53.402 mm/y for the entire ridge (Gale et al., 2013). The east-west-trending ridge has been strongly influenced by the Galápagos hotspot since the development of the ridge approximately 25 Ma. The average rate of magma supply, ridge thickness, and axial ridge elevation all increase with proximity to the hotspot (Colman, 2016).

Prior work by Haines (2016) proposed multiple mechanisms of magma evolution along the Galápagos Spreading Center (GSC) from an analysis of the pressures and temperatures of magma crystallization. The variability of these pressures and temperatures correlated to offsets along the GSC, allowing for the GSC to be segmented according to these offsets. To analyze trace element variation with respect to changing pressures and temperatures of partial crystallization, the defined segments were adapted from Haines' study (Figure 2).

The research outlined herein used trace element geochemistry to constrain the processes of magma evolution prior to eruption along the GSC. The goal of this research was to construct a comprehensive model of the magma plumbing systems feeding the ridge through the analysis of major and trace element geochemistry combined with the findings of Haines' research on the pressures and temperatures of magma crystallization.

GEOLOGIC SETTING

Geologic Setting

The Galápagos Spreading Center (GSC) is an intermediate spreading ridge system located ~1000 km due west of Ecuador and ~200 km north of the Galápagos Islands that separates the Cocos and Nazca Plates. Spreading rates vary along the GSC with systematically increasing rates from West to East. The E-W trending ridge runs ~2100 km from 101.8°W to 82.8°W, terminating at the East Pacific Rise and a N-S striking transform fault respectively. The Galápagos hotspot is located beneath the Galápagos Islands, with a proposed center at 0.8°S, 90.5°W. Over the past 5 Ma the GSC has migrated northwards while being detained by the Galápagos hotspot, seen by numerous ridge jumps (Herbrich, 2016). The ridge is of petrologic and geodynamic interest because it is offset by transform faults and passes close to the Galápagos Islands (Haines, 2016).

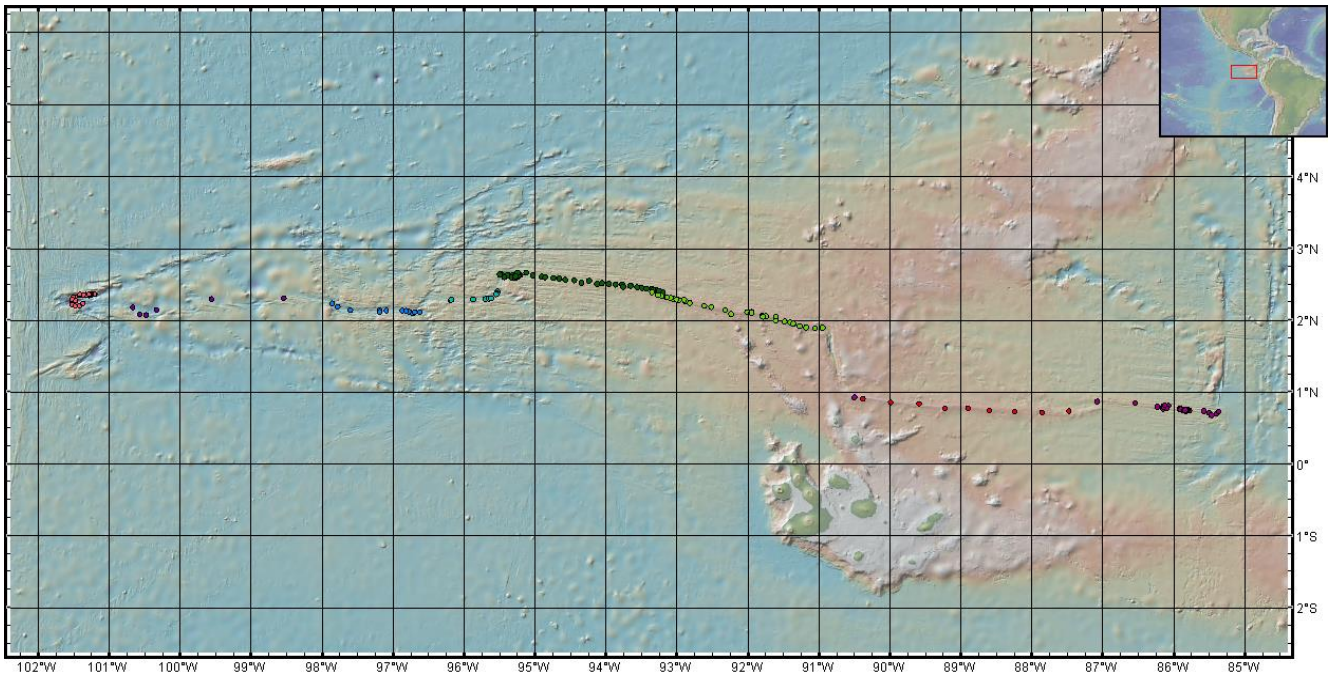

Figure 1: Map of the Galapagos Spreading Center with data samples (PetDB, 2017) indicated by colored points. The map was made with GeoMapApp (3.6.3).

METHODS

Trace elements, by definition, compose a small fraction of any system but provide geochemical and geological information out of proportion to their abundance. Trace element concentrations are of interest because (1) variations in trace element compositions are considerably greater than major oxide variations; (2) there are far more trace elements than major elements in any system; (3) trace elements are sensitive to processes to which major elements are insensitive; (4) trace element compositions in the mantle are quite variable thus providing chemical fingerprints of disparate magma reservoirs; and (5) trace elements obey Henry's Law relating dissolved gases in liquids to the partial pressure of the liquids (White, 2010). Therefore, trace element concentrations can provide insight to the natural processes driving the evolution of magmas erupted along mid-ocean ridges.

Prior work by Haines (2016) proposed multiple mechanisms of magma evolution along the Galápagos Spreading Center (GSC) from an analysis of the pressures and temperatures of magma crystallization. The variability of these pressures and temperatures correlated to offsets along the GSC, allowing for the GSC to be segmented according to these offsets. To analyze trace element variation with respect to changing pressures and temperatures of partial crystallization, the defined segments were adapted from Haines' study (Figure 2).

Data taken from the compilation of Mid-Ocean Ridge Basalt (MORB) analyses (PetDb, 2017) were used to examine geochemical variations in basalts erupted along the ridge. This database includes data for major oxides, trace elements and isotopes for each sample along with latitude, longitude and water depth. Using Microsoft Excel, 7,117 whole rock sample analyses were compiled and subsequently filtered to eliminate duplicate samples, samples with incomplete major oxide and trace element analyses, and samples collected outside of the study area. A dataset of 676 sample analyses resulted after the removal of samples with incomplete major oxide or trace element compositions and samples acquired away from the ridge. The resulting dataset was used for interpretations made in this thesis. The samples were sorted according to ridge offsets along the GSC. The ridge segments, primarily defined by longitudinal location, were alphabetically denoted from the westernmost segment (A) to the easternmost segment (K)(Table A1). Ridge segments G and J were discarded due to insufficient sample sizes, containing one and five samples respectively. Segment K was discarded due to the sample size and large offset distance from the other ridge segments. Major oxides were normalized to 100 wt.%, while trace elements were normalized to the average Normal Mid-Ocean Ridge Basalt (NMORB) composition defined by Gale et al. (2013). Rare

earth elements were normalized according to the Cl-chondrite composition distinguished by McDonough and Sun (1995).

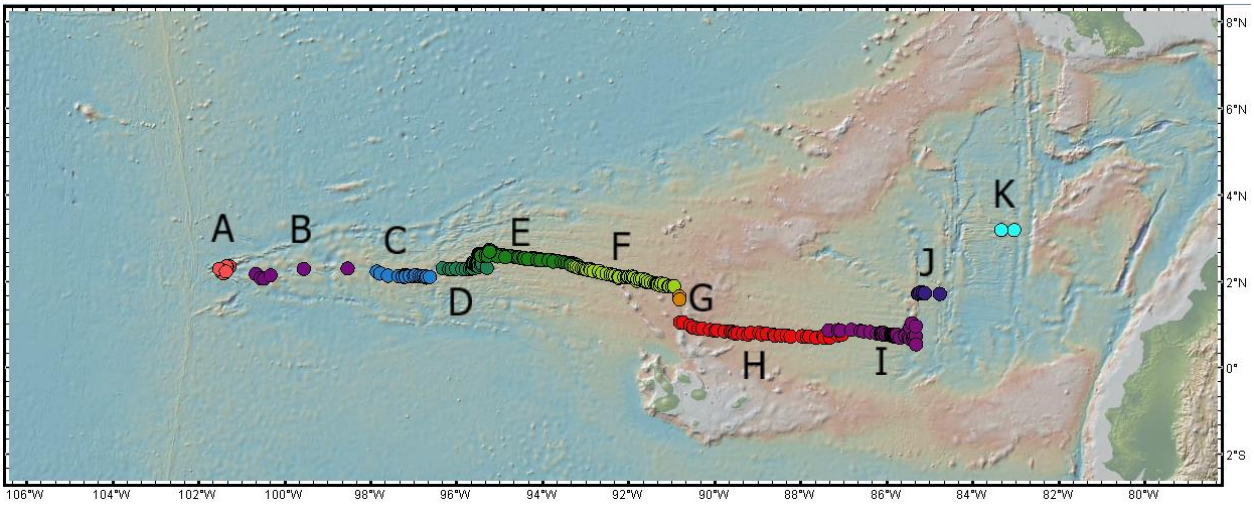

Figure 2: Map of the GSC ridge segments labeled and data samples (PetDB, 2017) indicated by colored points. Map was made with GeoMapApp (3.6.3)

The statistical and plotting software package COHORT was used to examine the extent to which geochemical variations are consistent with crystallization and to identify the effects of crust-magma interaction. Spider diagrams were used to determine trace element enrichments or depletions compared to an average NMORB composition. Trace element concentrations were normalized to the NMORB composition (Gale et al., 2013). Twenty-nine trace elements were plotted for each sample in a ridge segment. Elements on the spider diagram were arranged according to their incompatibility. The partition coefficient (D) – a function of temperature, pressure, and composition of involved phases – for an element defines its affinity for preferential partitioning into the melt or solid phase. Elements with $D<<1$ are incompatible whereas elements with $D \geq 1$ are compatible (Winter, 2010). Incompatible elements are those that partition into a melt phase when the mantle undergoes partial melting. In basaltic and ultramafic rocks, cationic tetrahedral sites – typically occupied by Si, Al, Fe^{3+}, Ti^{4+} – and octahedral sites – typically occupied by Ca, Mg, Fe, or Na – are energetically unfavorable for substitutions of incompatible trace elements. Compatible trace elements, conversely, substitute into cationic sites favorably and remain in residual minerals as melting occurs (White, 2010). The most incompatible elements are positioned on the left of the diagram with increasing compatibility to the right. Large-ion-lithophile (LIL) elements – Cs, Rb, Ba, and Sr – have the highest incompatibility thus they are located the furthest left. Compatible trace

elements – Cr and Ni – constitute the far right. Bulk mantle compositions were constrained using ratios of normalized trace element compositions with contrasting compatibilities, such as Rb/Y_N (Table A1). The degree of incompatible trace element enrichment or depletion varies locally within ridge segments. Thus, bulk mantle compositions are based on the aggregate ridge segment compositions. A normalized ratio of 1 represents an average NMORB composition. Ratios deviating from 1 indicate an enriched MORB (EMORB) or a depleted MORB (DMORB). The sign of the slope of a line connecting the aggregate Rb_N and Y_N compositions shows incompatible trace element enrichment ($Rb_N>Y_N$, negative slope) or depletion ($Rb_N<Y_N$, positive slope) (Winter, 2010). Plots of K_2O vs. TiO_2 and P_2O_5 were used to detect evolutionary processes other than partial crystallization. Plots of trace element compositions versus longitude were used to investigate systematic variations of magma composition in relation to plume proximity. Plots of trace element ratios, such as La/Sm_N and Mo/Ce, versus longitude were used for rapid visualization of changing magmatic evolution processes, including regions of mantle plume influence on magmas. Major oxide versus major oxide plots from Haines (2016) were used to identify evolutionary processes aside from theoretical compositions resulting solely from crystallization. Analysis of these plots, in conjunction to one another, were used to constrain the processes of magma evolution along the GSC.

.

RESULTS

Trace Elements

Spider diagrams show a depleted MORB (ridges A–E) and an enriched (ridges E–I) mantle source transitioning at approximately 95.5°W and 87.1°W (Figures 3 and 4). Segment A contains several sample compositions from an enriched mantle source. These enriched samples are clustered where the GSC terminates at the Eastern Pacific Rise. Regardless of the anomalous enriched compositions, segment A is mostly a DMORB (Rb/Y_N= 0.6361). Segments B, C, D, part of E (95.4972–95.4925°W), and I are also depleted in incompatible trace elements relative to NMORB [B (Rb/Y_N= 0.084); C (Rb/Y_N= 0.5254); D (Rb/Y_N= 0.6748); E (Rb/Y_N= 0.16793); I (Rb/Y_N= 0.9553)]. Segments E (95.4712-93.205°W), F, and H exhibited melt compositions enriched in incompatible trace elements relative to NMORB [E (Rb/Y_N= 1.731); F (Rb/Y_N= 3.537); H (Rb/Y_N= 4.666)]. The GSC can be split into 3 distinct regions according to the underlying bulk mantle composition: depleted western, enriched central, and depleted eastern segments. The changing regions of melt compositions, from depleted to enriched to depleted, may be indication of multiple magma plumbing sources feeding the spreading center.

Further analysis of spider diagrams shows slight negative Eu anomalies in conjunction with substantial negative Sr anomalies, primarily along the central and eastern regions of the GSC (ridges E-I, Figures 2 and 3). The anomalies demonstrate the importance of plagioclase crystallization in magma evolution (Winter, 2010).

Trace elements are very sensitive to fractionation processes throughout the magma's evolution. When single trace element abundances are plotted versus longitude, the fluctuations of trace element concentrations normalized to NMORB (Gale et al., 2013) help identify magmatic evolution processes responsible for crustal creation at divergent spreading centers. A plot of the compatible trace element, Cr_N, concentration along the GSC (Figure 5) shows three areas where the concentration is below that of a NMORB. Cr_N is depleted from approximately: 101.6–101.2°W along segment A, 94–86.5°W across segments E-I, and east of 86.4°W on segment I. Depletions of Cr signal that early crystallization of olivine and pyroxene have occurred.

Depleted compatible trace element compositions among samples suggest a late stage melt that had time to crystallize compatible elements out of the liquid. On the other hand, magmas of late stage melts may have spent a longer time in a chamber at any depth, thus having had ample time to evolve to extreme compositions late stage melts have had sufficient time to incorporate

incompatible trace elements into the melt.

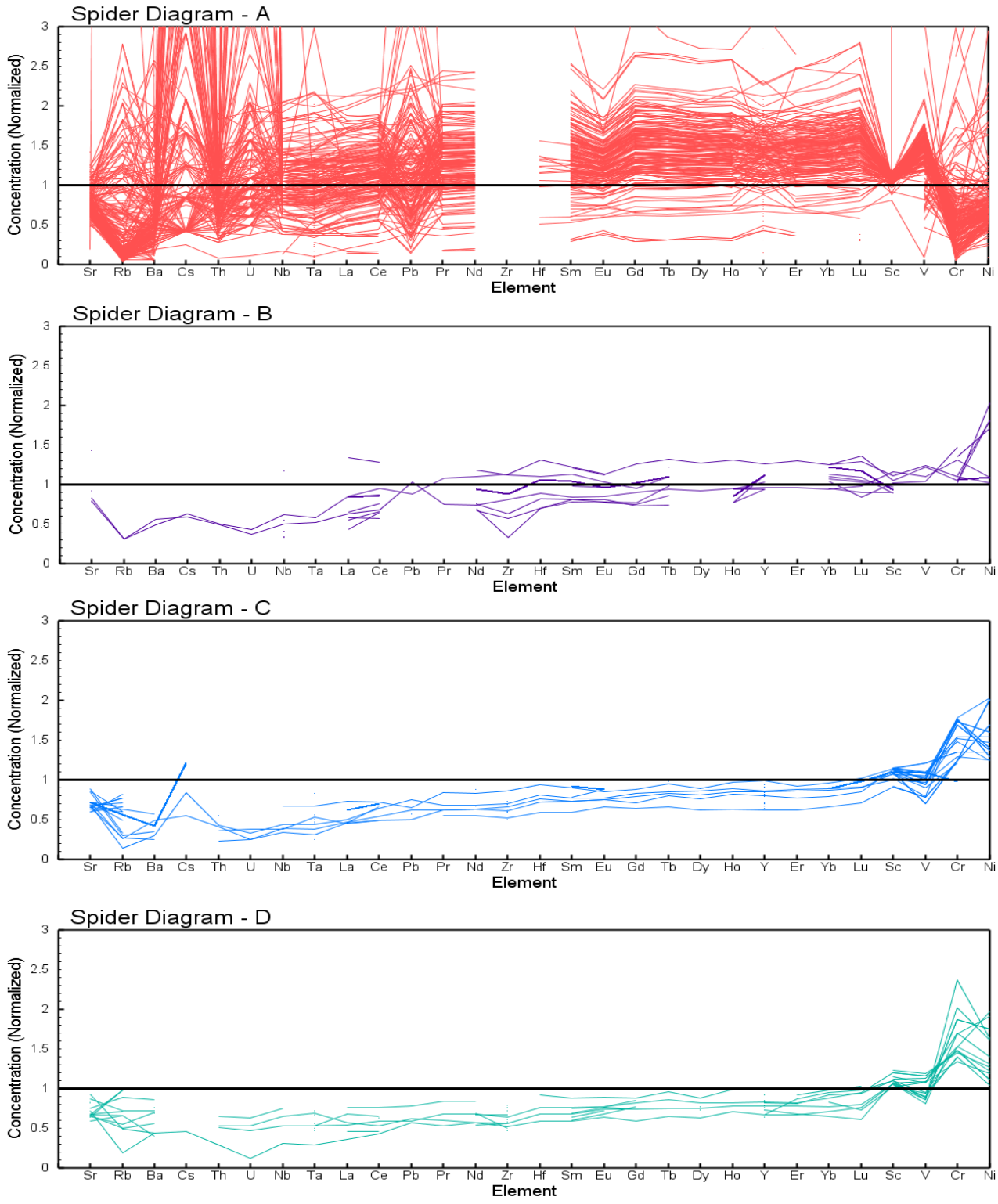

Figure 3: Normalized TE concentrations of 29 elements for individual GSC segments. Each line is from a single sample. Spider diagrams show a depleted MORB (A–E) and an enriched MORB (E–I) mantle source switching at ≈95.5°W. Mantle composition indicated by ratio of TE's with contrasting compatibilities (Rb/YN).

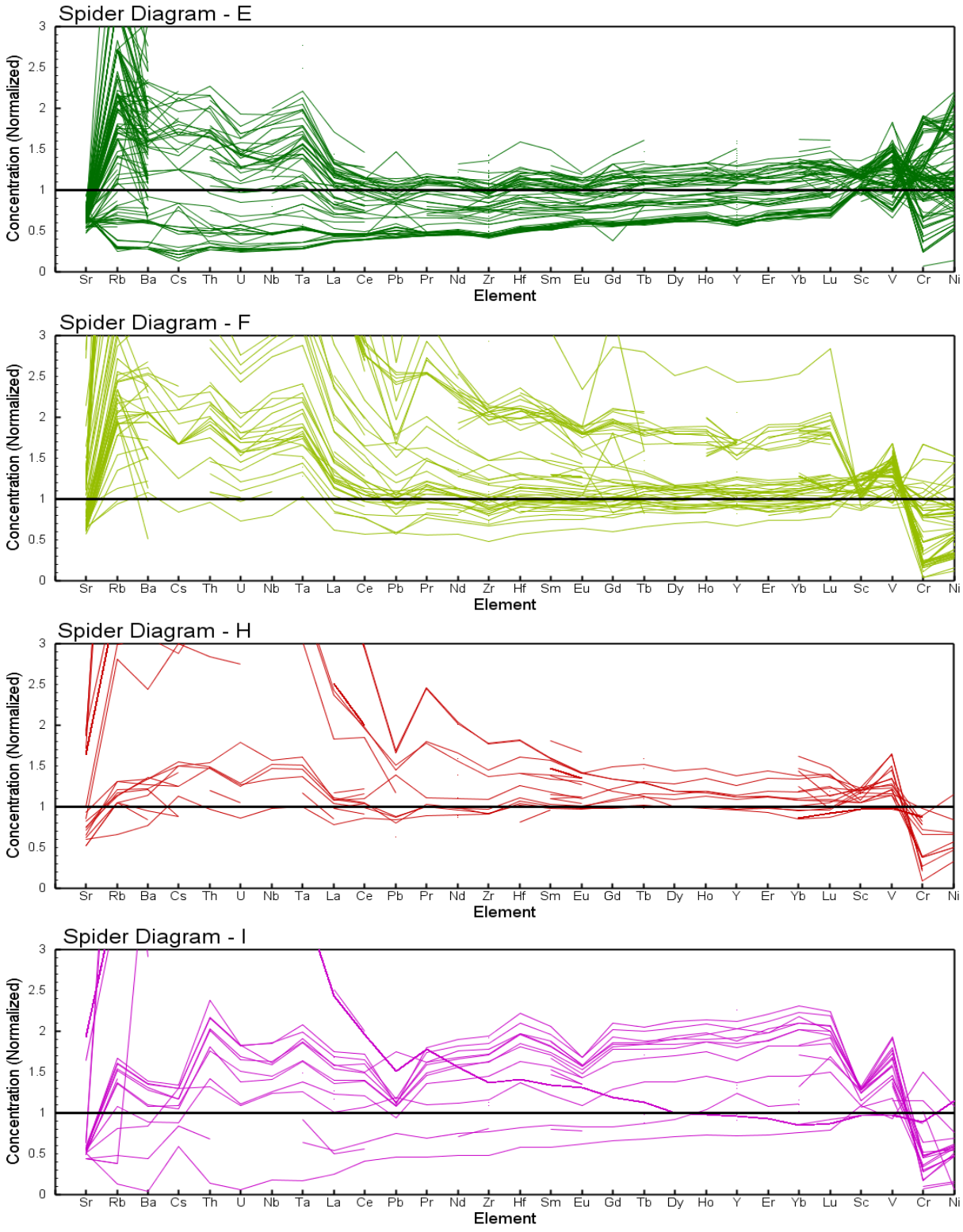

Figure 4: Spider diagrams for GSC ridge segments E, F, G, and H. Segment E displays two trends – an enrichment and a depletion. Both trends are isolated in the Appendix. Segments J, K, and L were discarded due to insufficient sample size.

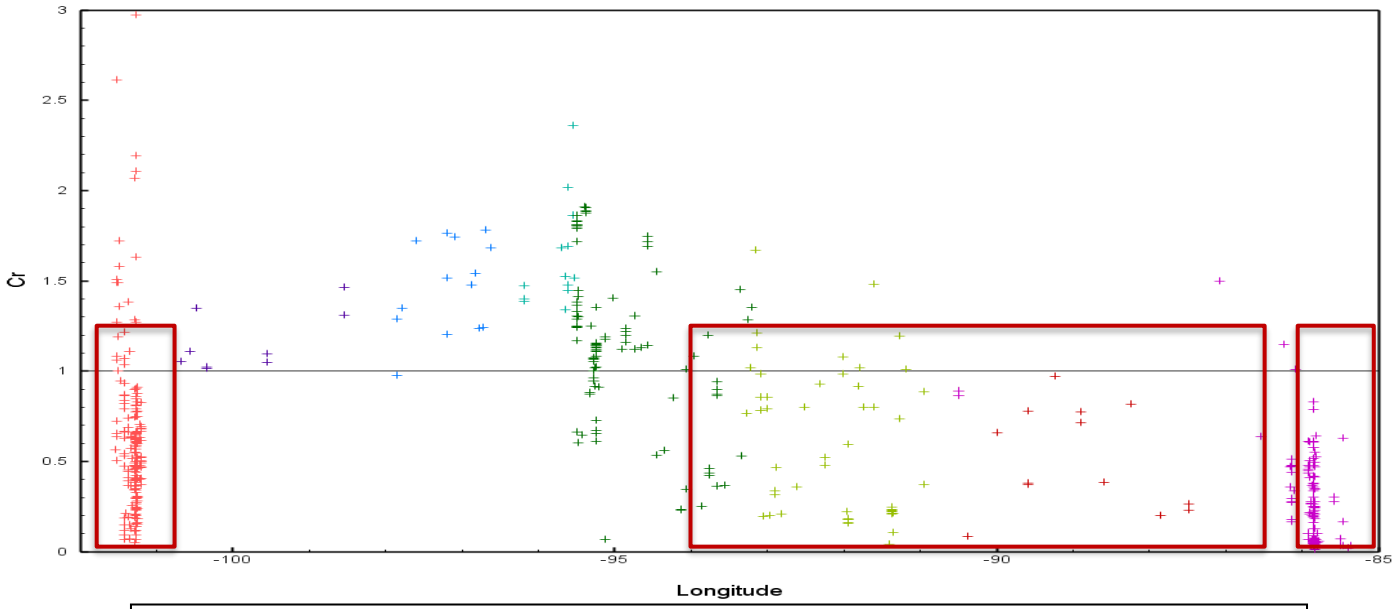

Figure 5: Cr concentrations normalized to NMORB plotted by longitude. Red boxes show regions where Cr_N drops below the NMORB concentration, indicating early crystallization of olivine and pyroxene has occurred.

Sr_N, an incompatible large-ion-lithophile element, exceeds the NMORB concentration on segment A (~101.25°W) and from ~92.5-89.6°W (segments E-I) reaching more than triple the concentration of the NMORB average at 90.5°W (Figure 6). Concentrations of the high field strength element, U_N, surpass the NMORB concentration along ridge segment A at ~101.25°W, throughout ridge segments E-I from 95.5-87.4°W and 86.4–85.37°W (Figure 7).

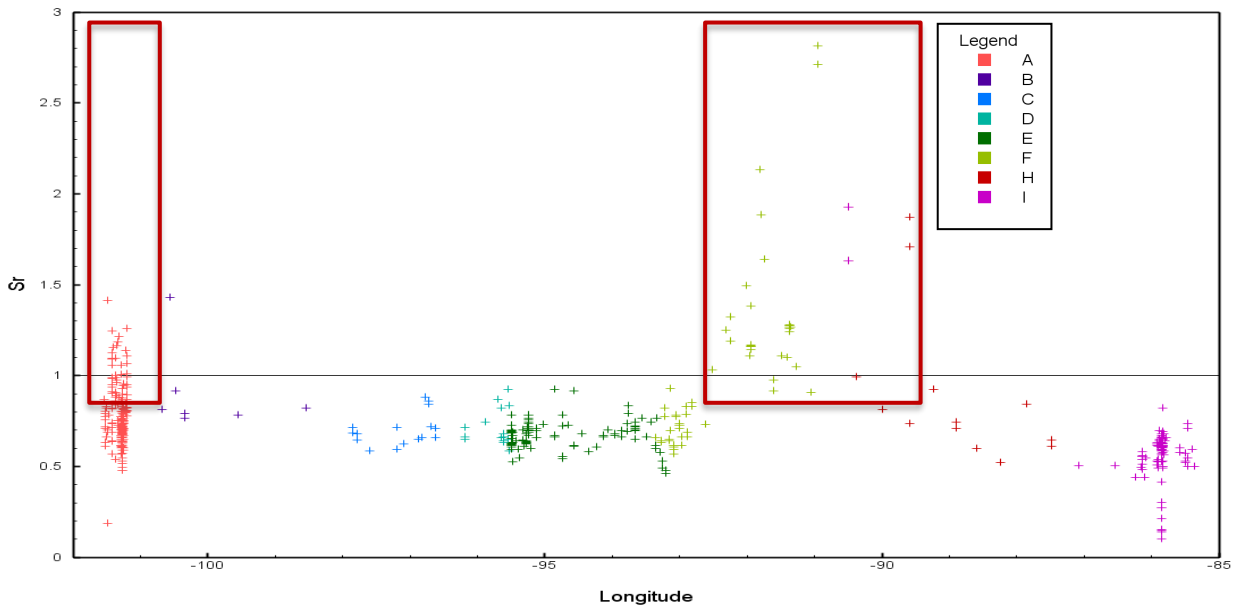

Figure 6: Sr concentrations normalized to NMORB plotted by longitude. Red boxes show regions where Sr_N exceeds a NMORB concentration.

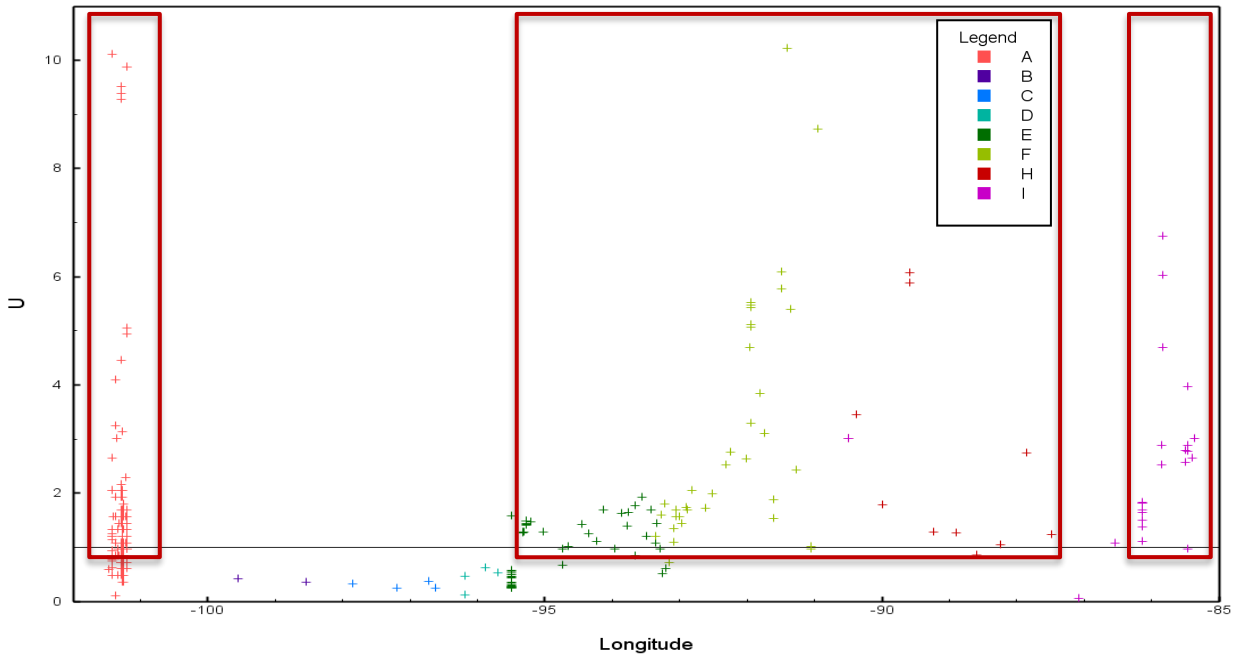

Figure 7: U_N concentrations normalized to NMORB plotted against longitude. Red boxes show regions where U_N exceeds a NMORB concentration.

Incompatible trace element ratios are typically less indicative of fractional crystallization and partial melting than absolute abundances, especially if their incompatibilities are alike. When extensive melting has occurred, the ratio of two incompatible trace elements in a melt will resemble that ratio in the magma source. Ergo, ratios of trace elements are often more informative than absolute abundances (White, 2010). Canonical ratios reported by Kelley et al. (2013) were used to determine the extent of the plume influence on the GSC plumbing system. Ratios of Mo/Ce, Sb/Ce, Cd/Dy, W/U, Rb/Tl, and La/Sm_N (chondrite-normalized) vary in relation to plume proximity (Figure 8). La/Sm_N is greater than the NMORB ratio along segments A and E–I; corresponding to the same segments of the GSC where anomalous concentrations of U occur. Mo/Ce spikes above the canonical ratio at 95.5°W, ~86.5°W, and ~86°W, proximal to the proposed area of plume influence on magma evolution by Kelley et al. (2013). Mo/Ce is inversely correlated with La/Sm_N although both are good indicators of plume influence on the mantle source. La/Sm_N

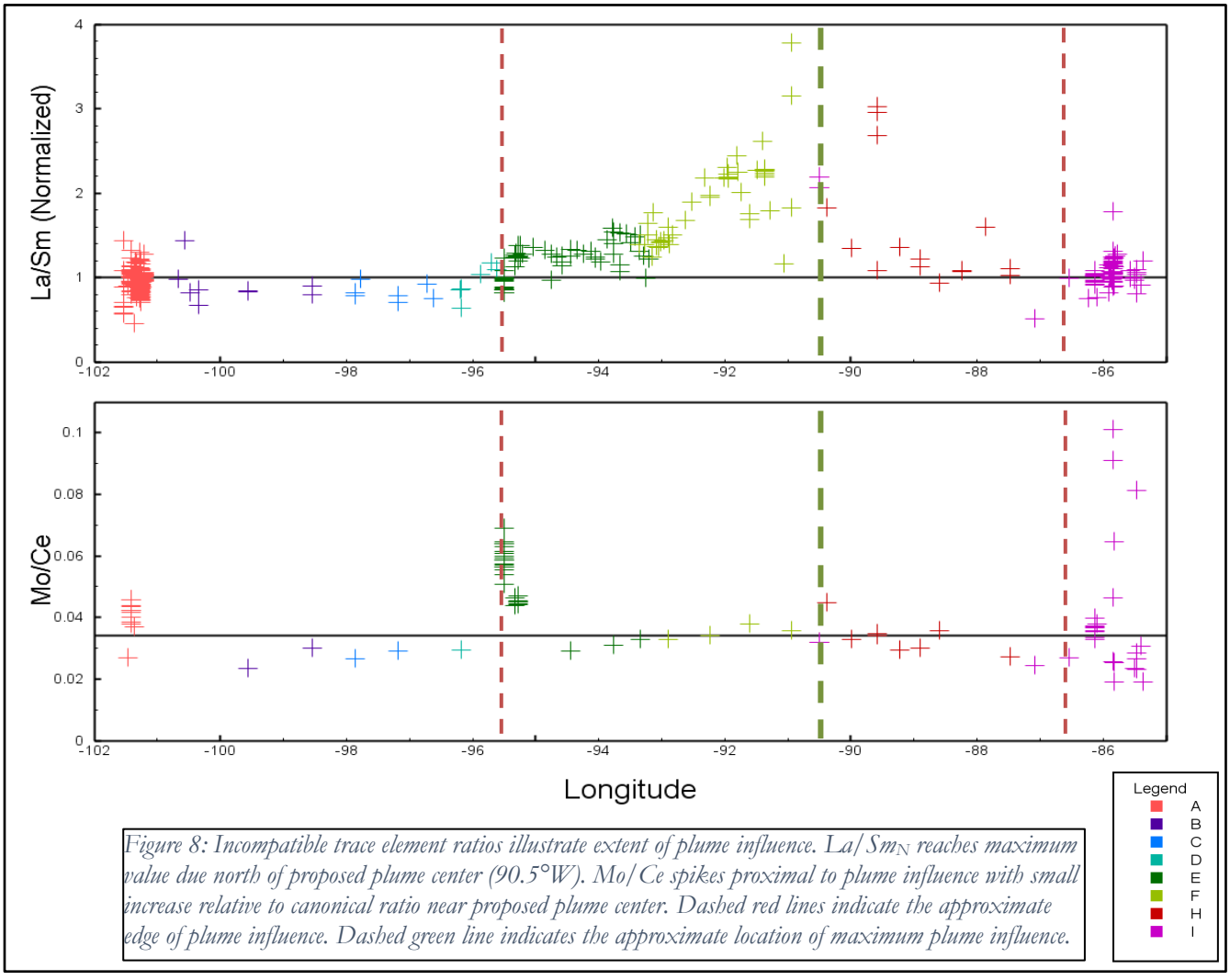

Figure 8: Incompatible trace element ratios illustrate extent of plume influence. La/Sm_N reaches maximum value due north of proposed plume center (90.5°W). Mo/Ce spikes proximal to plume influence with small increase relative to canonical ratio near proposed plume center. Dashed red lines indicate the approximate edge of plume influence. Dashed green line indicates the approximate location of maximum plume influence.

reaches its maximum value at the plume center (90.5°W) while Mo/Ce increases proximal to the plume ~95.5°W and ~86.5°W.

Major Oxides

Select plots of major oxides, both compatible and incompatible, were adapted from Haines (2016). Plots of K_2O vs. TiO_2 and P_2O_5 were utilized to identify elemental behaviors consistent with crystallization. Segment A displays a relationship between K_2O and P_2O_5 suggesting crystallization alone as the magma evolution process (Figure 9). All other ridge segments demonstrate relationships between major oxides indicative of multiple magma evolution processes across the ridge. Graphs of

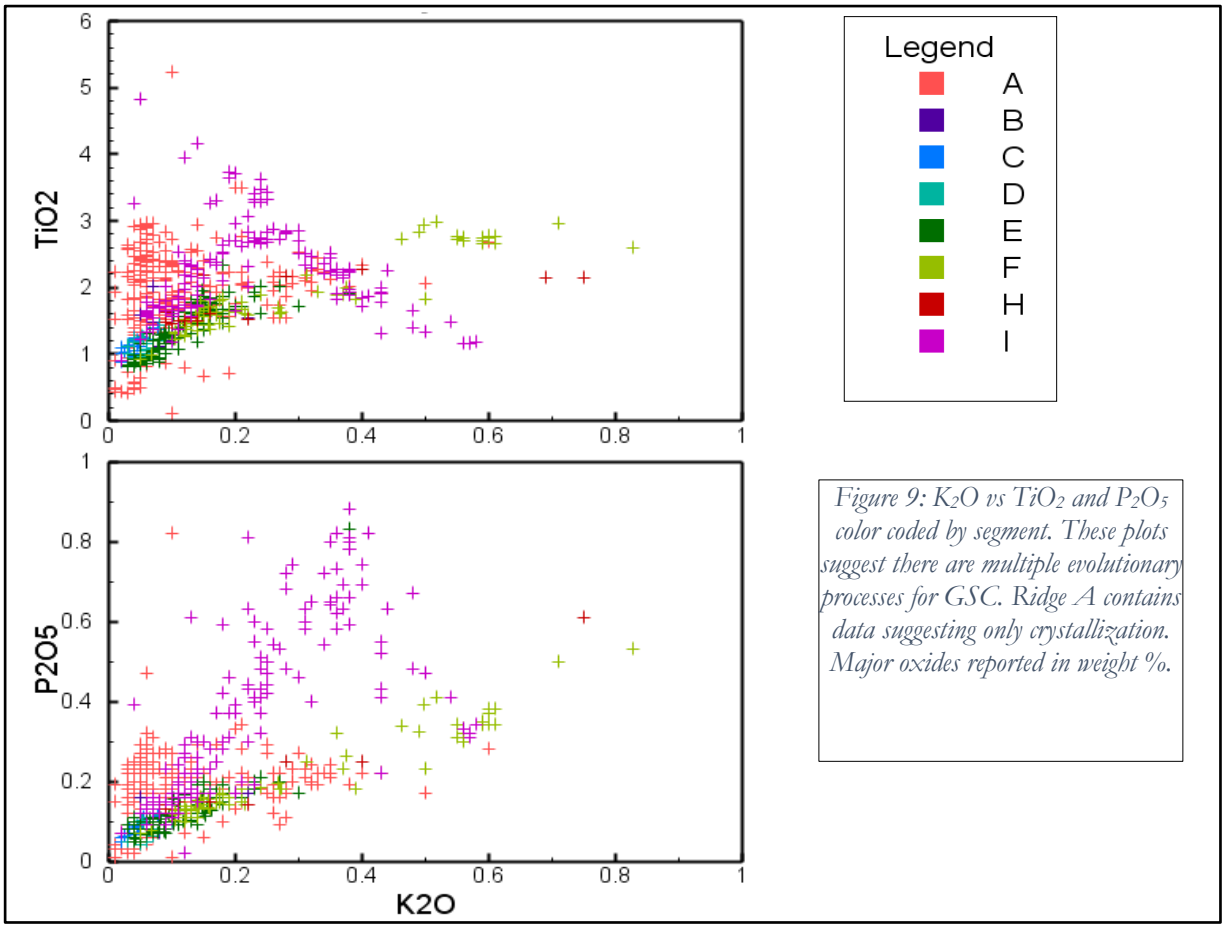

Figure 9: K_2O vs TiO_2 and P_2O_5 color coded by segment. These plots suggest there are multiple evolutionary processes for GSC. Ridge A contains data suggesting only crystallization. Major oxides reported in weight %.

MgO and K_2O vs. longitude (Figure 10) reveal the degree of magma evolution. High MgO concentrations indicate primitive, as seen in segments B–D, and high K_2O concentrations indicate evolved melts, as seen in segments A, E, F, and I. MgO behaves as a compatible element and substitutes into crystal lattices, whereas K_2O behaves as an incompatible element, always partitioning in the melt. Since these major oxides segregate according to their partition coefficients, we can

correlate samples composed of high K_2O concentrations with evolved melts and correlate samples composed of high MgO concentrations with primitive melts.

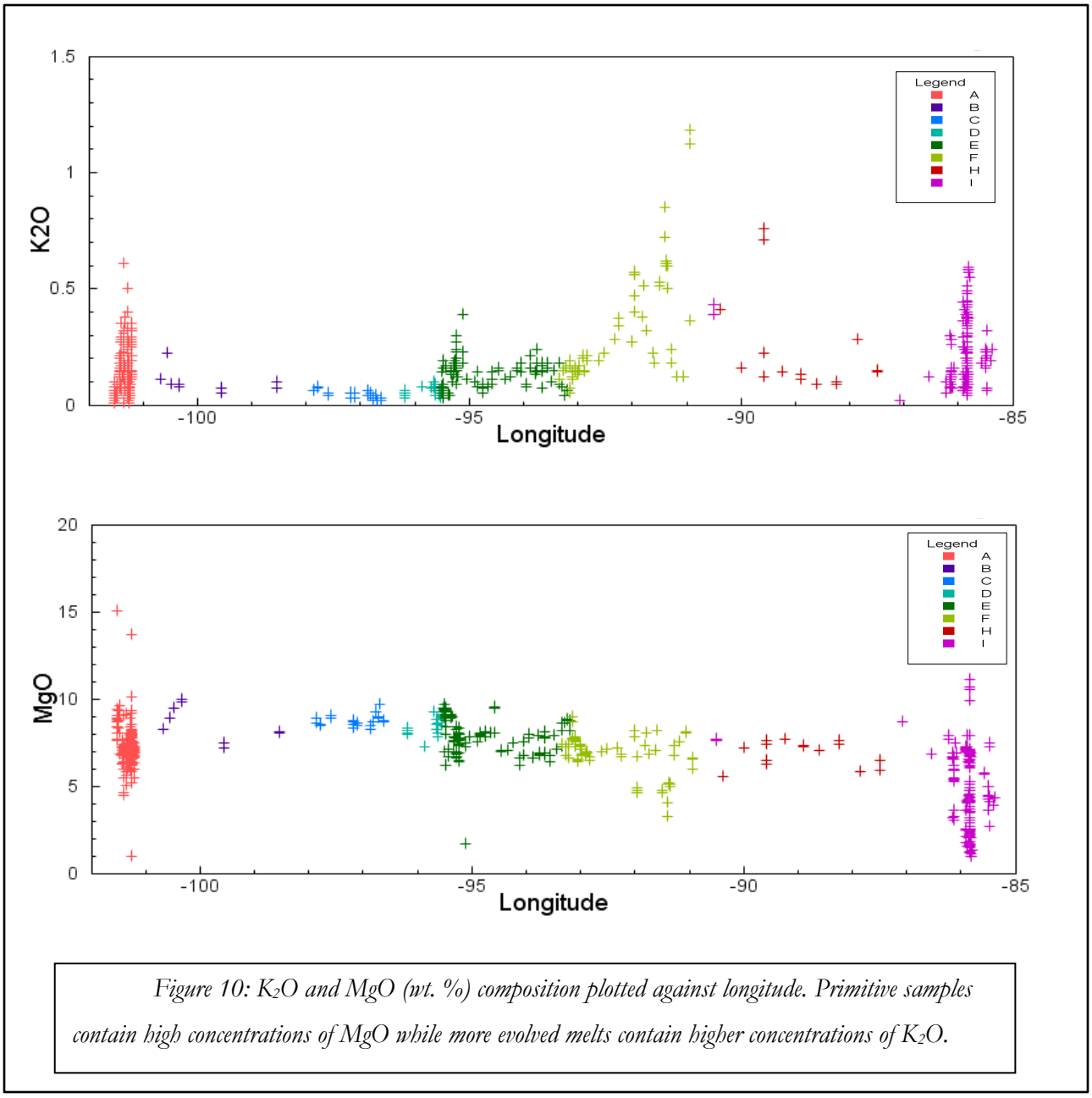

Figure 10: K_2O and MgO (wt. %) composition plotted against longitude. Primitive samples contain high concentrations of MgO while more evolved melts contain higher concentrations of K_2O.

Discussion

Trace Elements and Major Oxides

Normalized trace element spider diagrams show that magmas erupted along the GSC originate from at least three distinct mantle sources. The western most region of segment A contains elemental compositions similar to an EMORB but transitions to a DMORB away from the propagating tip to the east. Two possible explanations for this behavior are (1) the magma supply of segment A comes from a deep upwelled source region on the west side and a disparate relatively shallow region feeding the eastern portion of A and segments B-D or (2) the oceanic plate tectonics where the EPR meets the GSC enrich basalts in incompatible trace elements from a process such as crustal assimilation. Graphs of K_2O against major oxides (Figure 9) suggest the only process of magma evolution occuring along segment A is crystallization. Therefore, explanation 1 is more plausible but requires further study to make a definitive statement on the magma source region. Segments A and I exhibit basalts depleted in Cr, indicating early olivine or pyroxene crystallization, and a negative Eu anomaly, demonstrating an important role for plagioclase crystallization in magma evolution (Winter, 2010).

Spider diagrams of segments B-D exhibit a DMORB composition consistent with magmas derived from younger shallower region. Plots of K_2O vs. TiO_2 and P_2O_5 deviate from a 1:1 ratio suggesting multiple evolutionary processes of the magmas, most likely crustal assimilation.

Segment E contains samples consistent with derivation from both depleted and enriched mantle sources. Compositions west of 95.5°W are like basalts of segments B-D, suggesting a shared magma source. The change in mantle composition from depleted to enriched (95.5°W) correlates to the degree of plume interaction with the source region. Plume influenced areas have higher concentrations of incompatible trace elements. An EMORB composition between 95.5°W and 86.5°W is characteristic of a magma source highly influenced by a deep-sourced plume.

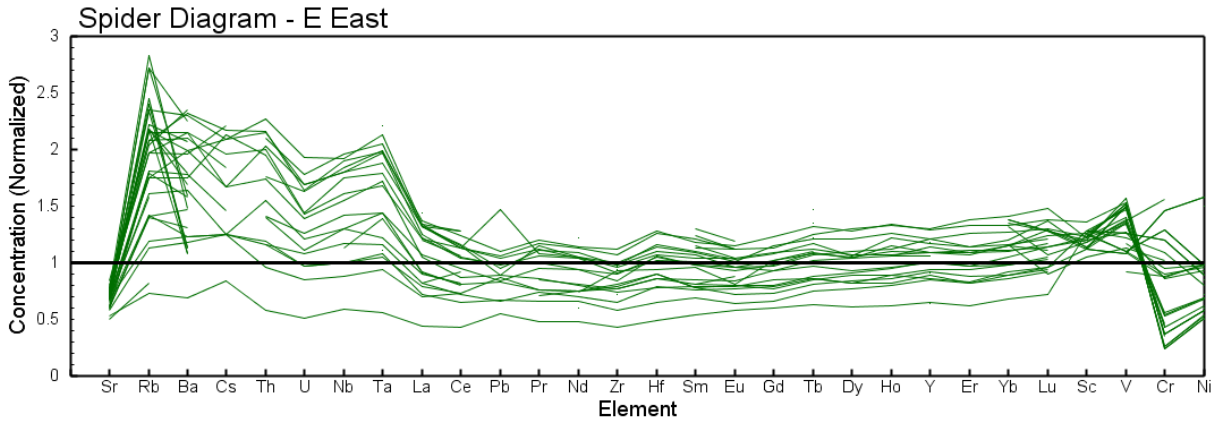

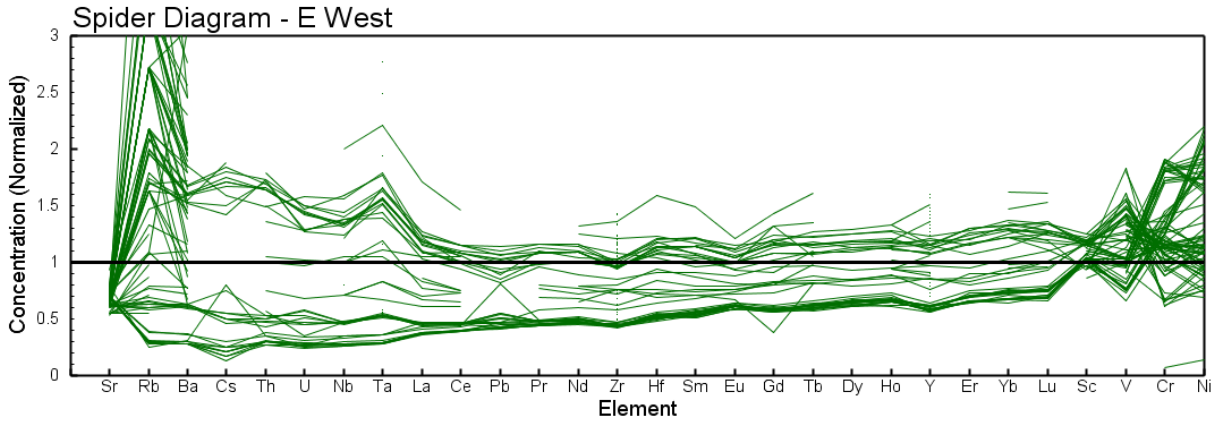

Figure 11: Spider diagrams from segment E split into two sub-segments. The eastern samples are enriched in incompatible trace elements. The western samples are depleted in incompatible trace elements, on aggregate.

Mo/Ce is inversely correlated with La/Sm_N although both are good indicators of plume influence on the mantle source. La/Sm_N reaches its maximum value due north of the proposed plume center (90.5°W) while Mo/Ce increases proximal to the plume (95.5°W & 86.5°W), confirming the breadth of the plume influence proposed by Cushman et al. (2004). Increased concentrations of Ba and Rb along these ridge segments coupled with small derivations from linear relationships between Ba vs. La and Ba vs. Nb suggest minor role of crustal assimilation in magma evolution (Figure 12).

The behavior of SiO_2 vs. MgO suggests magmas to the east of 86.5°W were influenced by evolutionary processes other than fractional crystallization, most likely crustal assimilation. SiO_2 compositions above 55 wt.% and high incompatible trace element concentrations in segment I indicate another distinct magma source for the GSC (Figure 13). Enrichments could be the result of a deep-upwelled magma plumbing system or from extensive crustal interaction near transform faults. These possibilities are speculative and require further study.

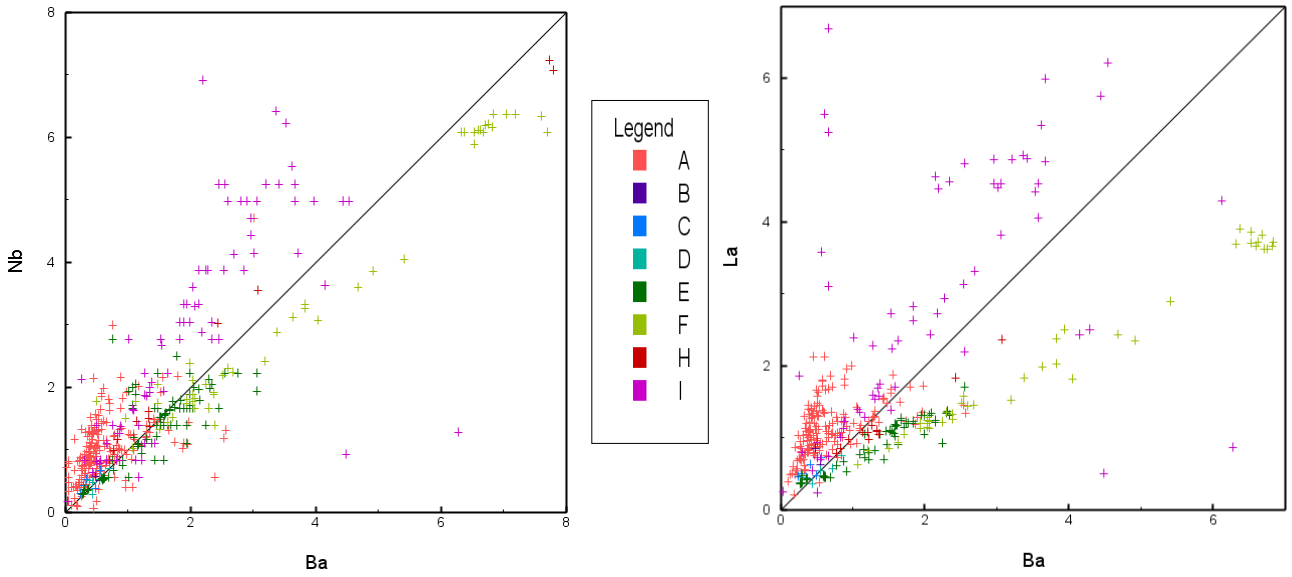

Figure 12: Ba plotted against Nb and La. All concentrations were normalized to a NMORB composition. Linear relationships between both elements suggest minor crustal assimilation occurring during magma evolution. The legend corresponds to both figures (12 and 13).

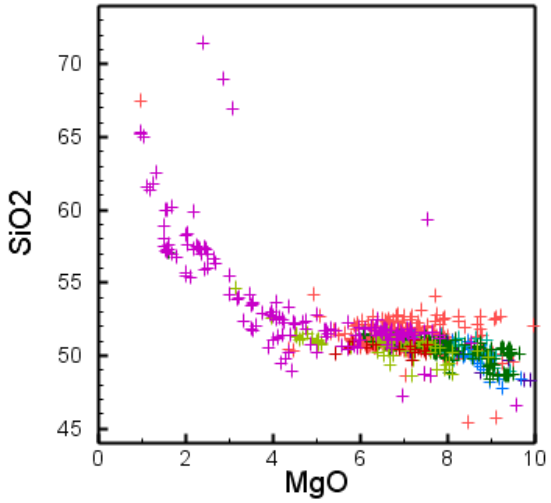

Figure 13: SiO_2 plotted against MgO (wt. %). Clustered samples indicate fractional crystallization as the primary evolutionary mechanism of magmas. SiO_2 concentrations above 55 wt. % may indicate a separate mantle source region for magmas erupted along segment I.

CONCLUSIONS

Multiple processes of magma evolution are in play at the Galápagos Spreading Center. Trace element geochemistry indicates fractional crystallization and crustal assimilation are the primary evolutionary processes of magmas derived from three separate magma source regions. Analysis of trace elements along with major oxide data provide evidence constraining the magma plumbing systems feeding the GSC. These include:

(1) The Galápagos plume effects the GSC between 95.5°W & 86.5°W with the maximum degree of influence at 90.5°W.

(2) Fractional crystallization occurs within the entire GSC. The role of fractional crystallization at the propagating tip and near eastern transform faults on the GSC is decreased. This is supported by marked Sr and Eu anomalies across the ridge, a proper relationship between MgO and SiO_2 between ridge tips, a linear relationship between La and Sm in areas uninfluenced by the plume, and a linear relationship between Hf and Zr along the entirety of the ridge.

(3) Crustal assimilation also occurs along the entire GSC. During crystallization, K_2O and TiO_2 (and P_2O_5) should vary in a 1:1 ratio. Most of the samples deviate from the ratio, suggesting that there was another evolutionary process of the magma. Plots of Ba and Rb versus longitude indicate the role of crustal assimilation varies along the ridge, with an increased role on the regions of plume-influenced ridge and at the eastern transform fault.

(4) Magmas erupted at the GSC evolved from different mantle sources. Sample compositions at 101.25°W, 95.4–87.4°W, and 85.37°W exhibit characteristics of a late stage melt. This is supported by decreased compatible trace elements with increased incompatible trace element compositions at these locales. Magmas of the GSC ridge

between 101.2–95.5°W exhibit characteristics of an early stage melt from a shallower mantle source.

(5) Plagioclase, olivine, and pyroxene play an important role in fractional crystallization along the ridge. Marked Eu anomalies demonstrate the importance for plagioclase crystallization in magma evolution while depletions of Cr indicate early olivine and pyroxene crystallization out of the melt.

RECOMMENDATIONS FOR FUTURE WORK

Further analysis of trace element data should be completed to better define magma source regions in the mantle. These can be compared with those established for other ridge systems.

Systematic variations in trace element abundances should be modeled to establish the relative roles of crystallization and assimilation in magma evolution. Trace element data will be combined with pressures calculated by Haines to better understand magma evolution along the GSC. Thin section analysis can provide additional evidence to support conclusions of the aggregated datasets.

REFERENCES CITED

CoHort Software, 2017, CoPlot: v. 6.450.

Colman, A., Sinton, J.M., and Rubin, K.H., 2016, Magmatic processes at variable magma supply along the Galapagos spreading center; constraints from single eruptive units: Journal of Petrology, v. 57, p. 981-1018, doi: 10.1093/petrology/egw032.

Cushman, B., Sinton, J.M., Ito, G., and Dixon, J.E., 2004, Glass compositions, plume-ridge interaction, and hydrous melting along the Gala´ pagos Spreading Center, 90.5°W to 98°W: Geochemistry, Geophysics, Geosystems, v. 5, doi: doi:10.1029/2004GC000709.

Gale, A., Dalton, C.A., Langmuir, C.H., Su, Y., and Schilling, J., 2013, The mean composition of ocean ridge basalts: Geochemistry, Geophysics, Geosystems, v. 14, p. 489-518, doi: 10.1029/2012GC004334.

Haines, K.A., and Barton, M., 2016, The pressures of partial crystallization along the Galapagos spreading center.

Herbrich, A., Hauff, F., Hoernle, K., Werner, R., Garbe-Schönberg, D., and White, S., 2016, A 1.5 Ma record of plume-ridge interaction at the Western Galápagos Spreading Center (91.400 – 92.000°W): Geochimica Et Cosmochimica Acta, v. 185, p. 141-159, doi: 10.1016/j.gca.2016.04.036.

Kelley, Katherine A., Kingsley, Richard, Schilling, Jean-Guy, 2013, Composition of plume-influenced mid-ocean ridge lavas and glasses from the Mid-Atlantic Ridge, East Pacific Rise, Galápagos Spreading Center, and Gulf of Aden: Geochemistry, Geophysics, Geosystems, v. 14, p. 223-242.

Macdonald, K.C., 2001, Mid-ocean Ridge Tectonics, Volcanism, and Geomorphology: Encyclopedia of Ocean Sciences, p. 1798-1813, doi: 10.1006/rwos.2001.0094.

Marine Geoscience Data System, 2017, GeoMapApp: v. 3.6.3.

McDonough, W.F., and Sun, S.S., 1995, The composition of the Earth: Chemical Geology, v. 120, p. 223-253, doi: 10.1016/0009-2541(94)00140-4.

PetDB Database, 2017, : www.earthchem.org/petdb (accessed 2016).

White, W.M., 2010, Oceanic Island Basalts and Mantle Plumes: The Geochemical Perspective: Annual Review of Earth and Planetary Sciences, v. 38, p. 133-160, doi: 10.1146/annurev-earth-040809-152450.

Winter, John D., 2010, Principles of igneous and metamorphic petrology: New York, Prentice Hall.

APPENDIX

Ridge Segment	Graphic Color	Longitude	Sample Size	$(Rb/Y)_N$	Average Spreading Rate (mm/yr)
A		101.53°W–101.204°W	236	0.6361	40.2893
B		100.672°W–98.54°W	9	0.084	41.65095
C		97.86°W–96.628°W	23	0.5254	46.10775
D		96.191°W–95.53°W	19	0.6748	48.34456
E		95.4972°W–93.205°W	126	-1.731	50.52824
F		93.353°W–90.95°W	71	-3.537	53.94524
G		90.821°W	1	N/A	N/A
H		90.5°W–87.48°W	17	-4.666	58.40358
I		87.08°W–85.37°W	155	0.9553	62.6245
J		85.27°W–85.12°W	5	N/A	64.1996
K		83.34°W–83.04°W	14	N/A	65.8755

Table A1: Segments as defined by Haines (2016). Sample sizes are post-trim. The average spreading rates are those reported by Gale et al. (2013).

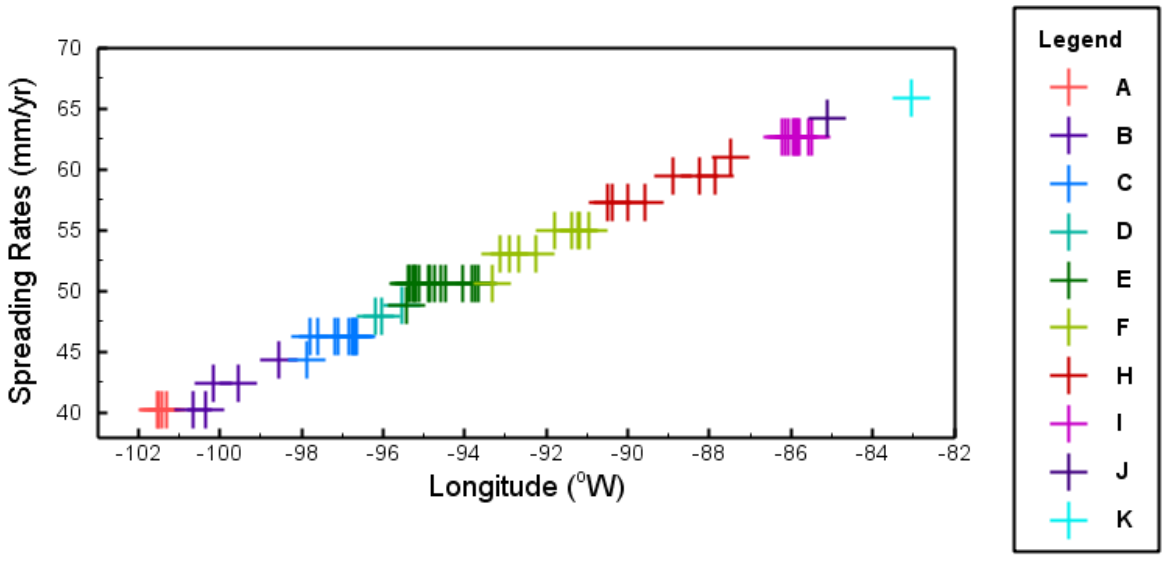

Figure A1: Gale et al. (2013) spreading rates plotted against longitude.

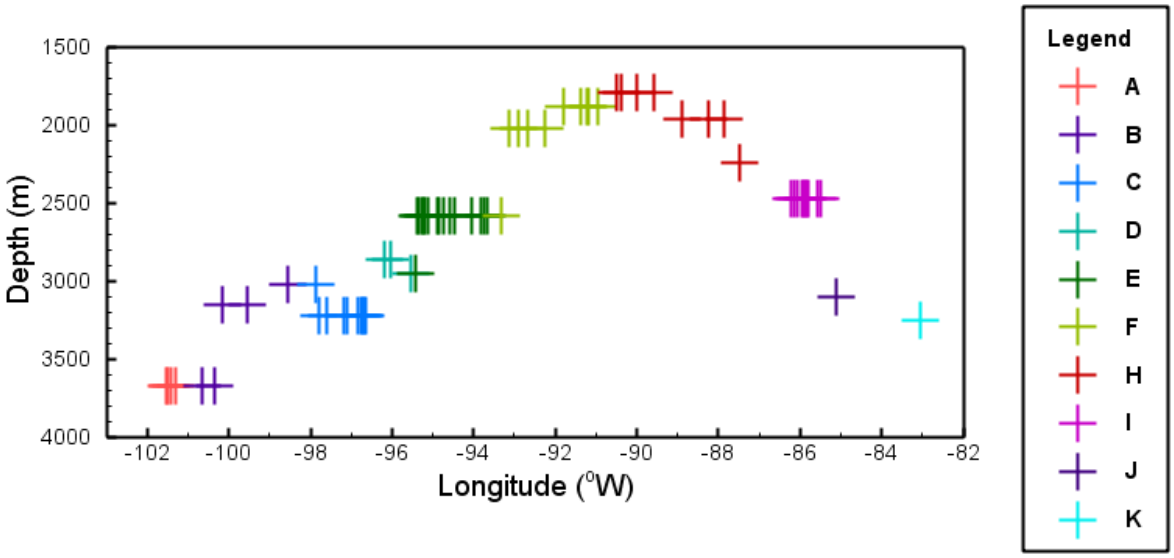

Figure A2: Ridge depths (Gale et al., 2013) plotted against longitude. Regions of increased plume influence are shallower than the average GSC ridge depth.

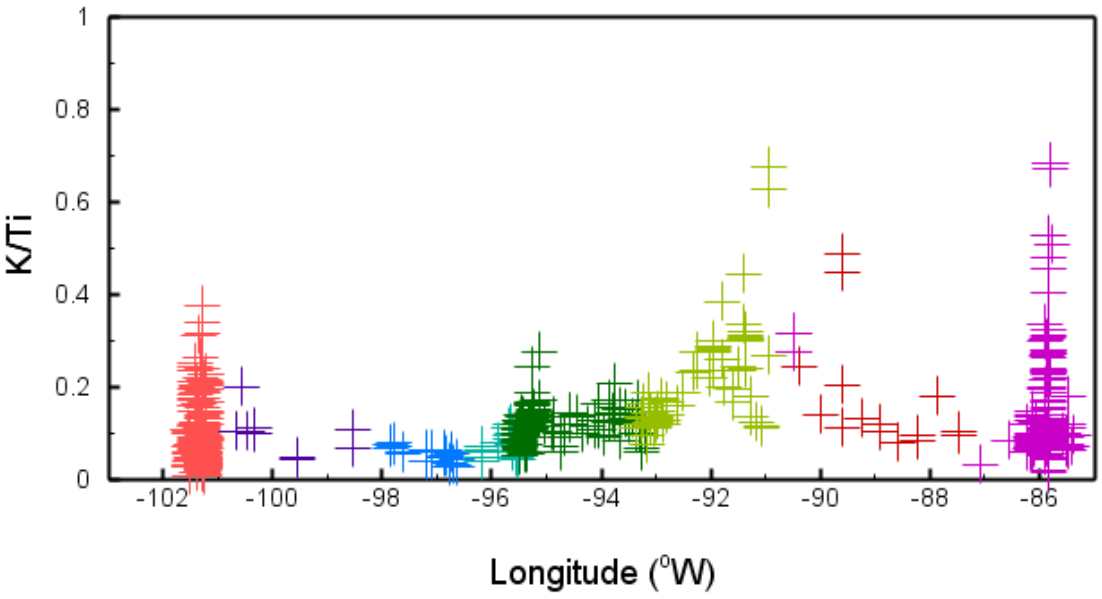

Figure A3: K/Ti ratios plotted against longitude. Major oxides used in the calculation were normalized to 100 wt. %.

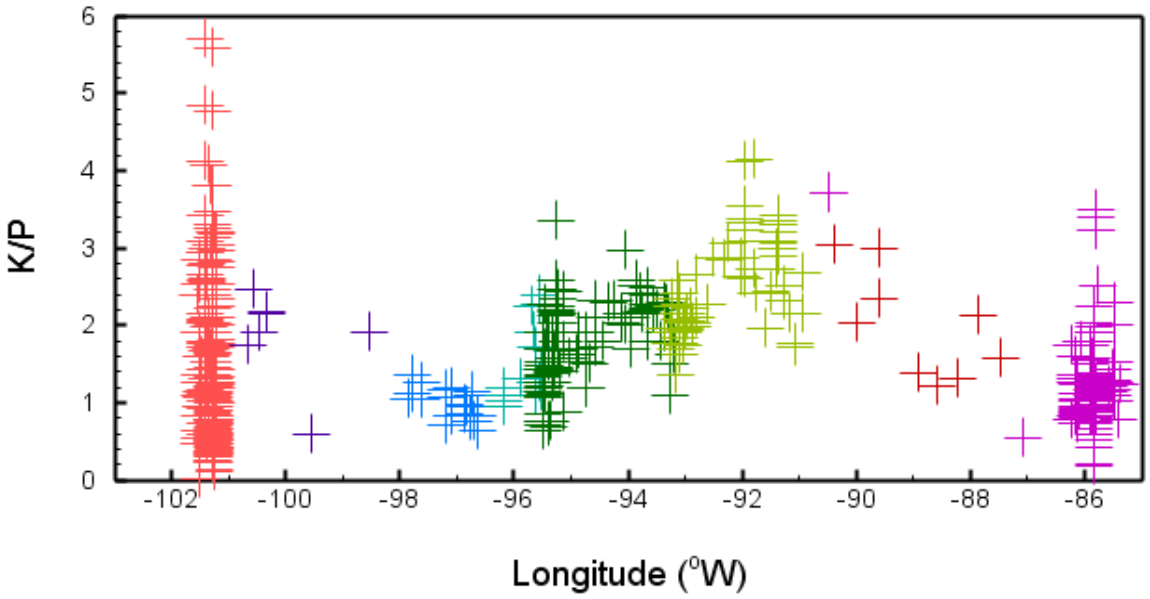

Figure A4: K/P ratios plotted against longitude. Major oxides used in the calculation were normalized to 100 wt. %.